ELSEVIER

Marine Geology 240 (2007) 77–97

MARINE GEOLOGY
INTERNATIONAL JOURNAL OF MARINE GEOLOGY, GEOCHEMISTRY AND GEOPHYSICS

www.elsevier.com/locate/margeo

Quantifying subaqueous slope stability during seismic shaking: Lake Lucerne as model for ocean margins

Michael Strasser [a,*], Sylvia Stegmann [b], Felix Bussmann [a], Flavio S. Anselmetti [a], Beat Rick [c], Achim Kopf [b]

[a] *Geological Institute, ETH Zurich, Universitätstrasse 16, CHN, 8092 Zurich, Switzerland*
[b] *Research Centre Ocean Margins (RCOM), University of Bremen, P.O. Box 330440, 28334 Bremen, Germany*
[c] *Dr. von Moos AG, Consulting geologists and engineers, Zurich, Switzerland*

Received 19 October 2006; received in revised form 1 February 2007; accepted 8 February 2007

Abstract

Lakes can be used as model basins to investigate subaqueous slope stability under static and dynamic loading conditions. This study combines geophysical, sedimentological and in situ geotechnical methods with limit equilibrium calculations in order to discuss (i) the geological and sedimentological processes acting on submerged non-deltaic lateral slopes in perialpine, fjord-type Lake Lucerne (Central Switzerland); (ii) their control on physical and geotechnical properties that eventually affect the subaqueous stability conditions and slope failure initiation, and (iii) the quantitative assessment of subaqueous slope stability. Three detailed case studies are presented to describe and quantitatively reconstruct stability conditions of slopes that failed during a well-documented historic earthquake in 1601 A.D. and during a prehistoric Late Holocene earthquake around 2220 cal yr BP (both $M_w > 6$).

Glacio-lacustrine sedimentation dominated by suspension settling from meltwater plumes and slight overconsolidation from ice-grounding during small readvances of a generally retreating glacier lead to a peculiar glacial-to-postglacial lithologic slope succession that eventually was buried by the Holocene sediment drape. During past earthquake shaking, the slopes that were stable under static loading conditions (factor of safety of 1.5–2) failed along planar sliding surfaces that developed at the lithological boundary between fine-grained, thinly-laminated, slightly underconsolidated cyclic plume deposits with low undrained shear strength values above and overconsolidated, glacially-deformed, glacio-lacustrine deposits with excessive formation pore pressure below. Measured in situ shear strength characteristics and sediment geometries were implemented into limit equilibrium models that allow for quantitative reconstruction of critical ground accelerations of past earthquakes in Central Switzerland. Results reveal seismic peak ground acceleration (PGA) of ~0.08 g and ~0.14 g for the historic 1601 A.D. M_w ~6.2 earthquake and the prehistoric, ~2220 cal yr B.P. earthquake, respectively. Additionally, results reveal that stability conditions change over relative short geological time scales because the postglacial sedimentation rate, which mainly controls the static weight of the slope sediment acting on the critical lithological boundary, turns out to be a key parameter in "charging" slopes susceptible to sliding.

Keywords: submarine landslides; slope stability; in situ measurement; sedimentation; limit equilibrium; paleoseismology

1. Introduction

Local instability of submerged sediment-covered slopes are common features in both marine and

* Corresponding author. Tel.: +41 44 632 6975.
E-mail address: strasser@erdw.ethz.ch (M. Strasser).

0025-3227/$ - see front matter © 2007 Elsevier B.V. All rights reserved.
doi:10.1016/j.margeo.2007.02.016

lacustrine environments and may have considerable catastrophic impact on offshore and coastal infrastructure (e.g. Shilts and Clague, 1992; Chapron et al., 1999; Locat and Lee, 2002; Boe et al., 2004; Lee, 2005). They originate from various processes such as erosion, rapid sedimentation, gas release or migration, earthquake shaking, diapirism, glacial and tidal loading, wave action, or clathrate dissociation (Hampton et al., 1996; Locat and Lee, 2002). Some of these geological processes act on the submerged slopes over longer time periods and are considered as causal factors whereas others are of instantaneous nature (e.g. earthquakes) and are thus referred to as short-term trigger mechanisms (Locat and Lee, 2002; Sultan et al., 2004). To understand past slope failure events and to eventually assess subaqueous landslide hazard, it is essential to reconstruct the pre-failure and failure conditions associated with subaquatic landslides (Leroueil et al., 1996), and also to quantitatively distinguish between long-term and short-term trigger processes.

Much of what is known today about subaqueous slope stability and hazard-related issues of underwater mass movements has been established from case studies during international campaigns along continental margins (e.g. Costa-Project (Mienert, 2004; and references therein) and Strataform-Project (Nittrouer, 1999; and references therein); see Locat and Lee (2002) for general summary) or from theoretical approaches using laboratory data or numerical modeling techniques (e.g. Biscontin et al., 2004; Azizian and Popescu, 2006). These studies present major advances in the quantitative assessment of submarine slope stability, but have also shown the challenges in determining in situ physical and geotechnical properties (e.g. shear strength and pore pressure) that are crucial for quantitative slope stability analysis. In the submarine environment, coring and in situ testing tools are expensive and critical subsurface structures along which failure occurred (or might occur in the future) are often located in depths inaccessible by those devices. Therefore, the acquired shallow subsurface data have to be extrapolated to critical depths (e.g. Urgeles et al., 2006) or the stability has to be assessed through normalized approaches (Lee and Edwards, 1986).

This study uses the lacustrine environment as a "model ocean" to quantitatively analyze subaqueous slope stability under static and dynamic loading. Due to their well-constrained boundary conditions, their smaller size and the possibility to be investigated on a complete basinwide scale, mass movements in lacustrine environments offer a series of advantages that make lake studies vital to improve our knowledge on marine processes. The three case studies of seismically-triggered slope failures in perialpine, fjord-type Lake Lucerne (Central Switzerland) presented here allow a quantitative discussion about the relationship between long-term causal factors and short-term trigger mechanisms. Methods developed for oceanographic and geotechnical investigations campaigns were utilized for site characterization. The limited sediment thickness covering the bedrock allows a complete in situ characterization of the slope-covering strata in failed as well as in stable areas. The combined geophysical, sedimentological, in situ geotechnical and limit equilibrium study presents a novel approach for slope stability assessment in the lacustrine environment, but resulting conceptual ideas give also new inputs in the context of larger slope instabilities occurring in particular in fjords or – more generally – on continental margins.

The primary objectives of the study are: (i) to understand the sediment dynamics and their control on the stability conditions along the lateral, non-deltaic slopes of Lake Lucerne; (ii) to quantify the sliding related key-characteristics (morphology, sedimentology, physical properties and in situ geotechnical parameters) of three earthquake-triggered slopes failures; and (iii) to quantitatively reconstruct seismic ground accelerations that affected the slopes at the time of failure.

2. Geological setting/Lake Lucerne

Lake Lucerne is a fjord-type, perialpine lake of glacial origin situated in Central Switzerland (~47°N, 8.5°E; 437 masl.; area = 116 km^2; Fig. 1). It consists of seven steep-sided sub-basins with relatively flat basin plains down to 220 m maximum water depth (Bührer and Ambühl, 1996). The substratum of Lake Lucerne is composed from S to N by the Helvetic Nappes, the Subalpine Molasse and the Plateau Molasse which are separated by the Northern Alpine thrust and Subalpine thrust, respectively (Fig. 1). The lake's complex shape and morphology result from efficient glacial erosion along weak zones associated with the regional geology. Past lake levels were slightly lower (~−9 m) and probably increased stepwise related to the growth of two opposing deltas in the outlet region near the city of Lucerne (Kopp, 1938).

This study concentrates on the lateral non-deltaic slopes of the external Chrüztrichter and Vitznau basins (Figs. 1 and 2) that are separated from the major deltas by sills formed by submerged moraines (Hantke, 2003). The three discussed study sites (i.e. the Weggis, St. Niklausen and Chrüztrichter sites) are located north of the Northern Alpine Front in areas with a molassic substratum consisting of sandstones and conglomerates.

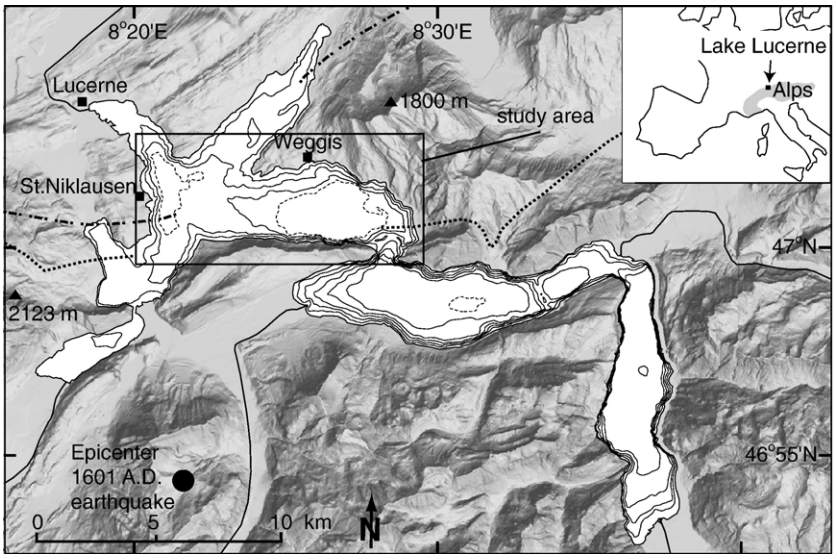

Fig. 1. Overview map of Lake Lucerne and its surroundings (shaded relief from 25 m digital terrain model, Swisstopo) showing the seven steep-sided sub-basins with flat basin plains. Bathymetric contour interval is 40 m. Dotted contour lines represent 20 m intervals and aim to clarify bathymetry. The rectangle indicates the study area and outlines location of subsequent Fig. 2. The dotted and dashed lines mark the Alpine and the Subalpine Front, respectively (see Section 2). Black circle in the SW corner of the map indicates estimated epicentral location of 1601 A.D. M_w ~6.2 Unterwalden earthquake (Schwarz-Zanetti et al., 2003; Gisler et al., 2004).

In the central region of the investigated sub-basins the bedrock is covered with an up to 120 m-thick, mainly glacial and glacio-lacustrine infill (Finckh et al., 1984). The majority of these sediments were deposited in a sub-glacial environment within relatively short time during the end of the last Glacial period. The Late Glacial basin sediments are comprised of thinly-laminated light gray to yellowish mud with frequent intercalated graded turbidite beds. The Holocene sediments consist of 5 to 15 m-thick, faintly laminated grayish to brownish mud with dark layers rich in organic matter and some intercalated graded turbidite beds (Schnellmann et al., 2006). Previous studies identified numerous mass-movement deposits related to a historic M_w 6.2 earthquake occurring in 1601 A.D. (Unterwalden Earthquake; Schwarz-Zanetti et al., 2003; Gisler et al., 2004) in the subsurface of Lake Lucerne (Siegenthaler et al., 1987, Lemcke, 1992; Schnellmann

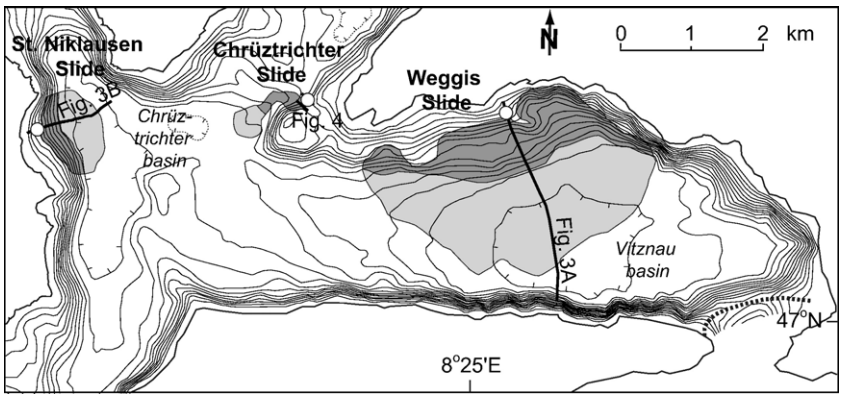

Fig. 2. Bathymetric map of Chrüztrichter and Vitznau basins showing the outline of the Weggis, St. Niklausen and Chrüztrichter Slides (see Fig. 1 for location of the map segment). Slide complexes are marked with grey shadings, whereby dark and light grey indicate erosional and depositional zones, respectively. Contour interval is 10 m. The bold dotted line in the SE corner indicates a major subaqueous sill and corresponds to an intermediate glacier front stage during deglaciation (Hantke, 2003). Bold lines indicate position of 3.5 kHz seismic profiles presented in subsequent figures. Open white circles give position of piston cores and in situ testing sites.

et al., 2002, 2005, 2006). Thirteen synchronous mass movements related to this event triggered a tsunami wave up to 4 m in height and a subsequent seiche wave that lasted for several days (Cysat, 1601; Schnellmann et al., 2002). In the deeper subsurface, five additional event horizons containing seismically-triggered synchronous mass movements were identified that have occurred in the last 15 000 yr. Schnellmann et al. (2006) provide a chronological catalogue of Late Glacial and Holocene mass-movement deposits and related subaqueous landslide scars in the two studied sub-basins. Slope failures are mostly characterized by translational movement and occurred in water depths ranging from 30–100 m. This study focuses on the source areas and on the pre-failure and failure conditions of three well-dated landslides, the deposits and depositional mechanisms of which are well constrained and for which strong seismic shaking was singled out as trigger mechanism (Schnellmann et al., 2005, 2006; Fig. 2).

3. Methods

3.1. Sub-bottom profiling

Closely spaced (~30–50 m grid spacing), single channel high-resolution 3.5 kHz seismic profiles (pinger source) were acquired in 2005 in order to refine the existing basinwide seismic data set (Schnellmann et al., 2006) in the areas of the three study sites. The source/receiver was mounted on a cataraft that was pushed in front of a small vessel. DGPS-positioning with a maximum error of ±2 m guaranteed accurate navigation. The digitally recorded data was processed using both a flat gain and band-pass filtering. Two-way travel time was converted to water depth and sediment thickness using a constant velocity of 1450 ms^{-1}. No migration was applied to the data because visual quality and readability is better in the non-migrated data and slope dip errors due to non-migration of the seismic sections are negligible (<2%).

3.2. Coring and laboratory analysis

At each study site, two Kullenberg-type gravity piston cores (Kelts et al., 1986), each 4.5–7 m in length, were recovered in the undisturbed slope-covering sediments adjacent to the failure scars. These cores provide material for both detailed characterization of sedimentological and physical properties, and for further geotechnical analysis on undisturbed samples. Additionally, at each study site 3 short gravity cores with a maximum length of 2 m were recovered along the failed slopes downslope of the failure scar.

The cores were logged in the Limnogeology Laboratory at ETH Zurich using a GEOTEK Multisensor Core Logger (MSCL), which measures Gamma Ray Attenuation bulk density, compressional wave velocity and magnetic susceptibility. Afterwards, cores were split for sedimentological description (macroscopically and using smear slide techniques; Rothwell, 1989; Kelts, 1998). Immediately after splitting, cores were photographed and natural water content measurements were performed by weighing 10 cm^3 of sediment before and after drying in an oven at 105 °C. On the freshly split sediment surface, undrained shear strength was measured perpendicular to bedding at ~15 cm intervals using a pocket vane shear testing device (Eijkelkamp). Atterberg limits were determined according to British Standards 1377 (Institute B.S., 1977) using a Casagrande apparatus. Grain size analysis were performed using laser diffraction techniques (Malvern Mastersizer Hydro 2000S) at ~10 cm intervals along the split core. Gravel clasts >2000 μm in the glacio-lacustrine sediments recovered at the bottom of the cores were removed by sieving prior to analysis, and clast diameters were estimated visually. Additionally, selected samples were analyzed for solid volume using a helium pycnometer device at the Rock Deformation Laboratory at ETH Zurich to derive grain density values. To characterize the consolidation history of the material, one dimensional consolidation tests (oedometer) were performed on two end-member lithologies from undisturbed samples taken from core 4WS05-K5 (Weggis site) at the Research Center Ocean Margins (RCOM), in Bremen. Specimens of 2 cm height and 5 cm in diameter were trimmed out of whole-round core samples and incrementally subjected to normal loads of up to 4 MPa.

3.3. In situ geotechnical testing

At the Weggis and St. Niklausen sites (see Fig. 2 for location) in situ geotechnical strength measurements were performed at ~50 cm intervals throughout the sediment profile. Both vane shear tests and Cone Penetration Testing (CPT; with pore pressure measurements) were performed to identify the in situ undrained strength profile. By using two independent methods the strength versus depth profile could be independently confirmed. Additionally, local induced excess pore pressure response could be measured and monitored to approximate the in situ pore pressure distribution.

The in situ vane shear tests were performed using a vane shear probe of 6.5 cm diameter (Geonor A/S) that was lowered in a casing mounted on an anchored platform. At each target depth the probe was extruded

carefully from the casing into the undisturbed sediment and rotated mechanically from the platform at constant rate (6°/min) until failure occurred. In the water saturated, fine-grained sediment, the hereby induced excess pore pressure does not have time to dissipate, thus the measured peak strength is inferred to be the in situ undrained shear strength ($c_{u\ in\ situ}$). The residual strength was then deduced from a consecutive test at the same interval. Only in the lowermost part of the section the measurements might be biased by the presence of gravels that occasionally block the vane shear device during rotation. Calibrating the system in the casing in the water above the lake bottom revealed negligible additional friction of the rotating rod. However, some inaccuracy results from the slight sediment disturbance when the probe is lowered. This results in underestimating the real in situ strength condition. Although the measurements were performed during calm periods with no wind-driven waves on the lake, minor waves from boats could not always be avoided so that early failure due to wave induced vertical movement of the vane shear device during the tests cannot always be excluded, potentially providing a second source for underestimating the actual in situ strength values.

A marine free-fall penetrometer from RCOM Bremen was used to measure strength and pore pressure in situ (Stegmann et al., 2006). The autonomous working tool consists of a standard industrial 15 cm^2 CPT cone and a pressure housing containing the power supply, data acquisition and an acceleration sensor. The tests were performed at the same location and at comparable depth intervals as the vane shear test. The CPT-instrument was lowered carefully from the anchored platform using a 4×4 car winch at the lowest possible rate (average rate ~2 cm/s) into the sediment, rested at each level for 10 min for pore pressure dissipation, and was then lowered to the next level, and so on. Insertion of the probe results in a compaction of the sediment, which generates an artificial excess pore pressure spike followed by pressure decay that approaches ambient values. By monitoring and evaluating the pore pressure dissipation after insertion, qualitative permeability conditions can be estimated (for details see Terzaghi, 1925). Additionally, these measurements provide confirmation that the strains induced during testing result in excess pore pressures and thus undrained loading at the test locations. Undrained shear strength ($c_{u\ in\ situ}$) was derived based on an empirical equation with the measured cone resistance during CPT-lowering using a standard cone factor (N_k), of 15 and 17 for normally consolidated clays and overconsolidated clays, respectively (for details see Lunne et al., 1997). Vane and cone penetration derived undrained shear strength cannot be directly compared because absolute values may differ significantly due to fundamental differences in the mechanical behavior between vane shearing and cone penetration (Lu and Bryant, 1997). Thus, the two independently measured $c_{u\ in\ situ}$ values are only considered for first order comparison of magnitude, but they can be used to identify characteristic strength versus depth trends.

3.4. Slope stability evaluation

2-D limit equilibrium slope stability analysis (for details see e.g. Duncan, 1996) were carried out using the commercially available software package Slide (Rocscience Inc.) that is widely used in geotechnical engineering for slope stability assessments under subaerial conditions, but allows for adaptation to the subaqueous environment. The program uses equal-width slices and allows for input of a slope profile, sub-bottom geometry of layers, their geotechnical properties and a predefined failure surface geometry. Additionally, a pseudostatic acceleration can be used to model the peak ground acceleration generated by earthquakes and to evaluate the seismic slope stability. This parameter assumes that the earthquake acceleration is applied over a significantly long period of time so that the induced stresses can be considered constant (Hampton et al., 1996). Thus, the dynamic response of the sediment cannot be taken into account. The output factor of safety (FS; i.e. the ratio between the resisting shear strength and the sum of all loading forces (mobilized shear stress)) is calculated using a combined General Limit Equilibrium (GLE)/Morgenstern–Price method (Morgenstern and Price, 1965; Fredlund and Krahn, 1977).

Two types of analysis were performed: (i) Deterministic back-analysis of seismically-triggered slope failures, and (ii) probabilistic limit equilibrium slope stability calculations. The back-analysis approach assumes FS = 1 at failure and tries to constrain the parameter combinations that could produce instabilities. Contrary to this deterministic method that uses one single constant value for each input parameter, the probabilistic approach considers variability and hence uses a mean and standard deviation value. Here, the input data samples are randomly generated using the Monte Carlo sampling method simulating the uncertainty and variability of each input parameters. FS is calculated for >1000 runs and model outputs reveal mean FS value of the modeled slope and the corresponding probability of failure (i.e. % of all analyses with FS < 1).

4. Data and results

Seismic interpretation and bathymetric evaluation allowed three target locations to be identified that are well suited for the purpose of this study (i.e. the Weggis, St. Niklausen and Chrüztrichter sites). They are characterized by (i) clear landslide scars related to known mass-movement events, (ii) undisturbed postglacial drape thickness adjacent to the failure scar <8 m (i.e., can be penetrated with coring and in situ testing probes), and (iii) water depth <40 m for in situ vane shear testing. In this section the analyzed morphological, sedimentological and geotechnical characteristics of this three studied lateral slopes that failed during past earthquakes are presented.

4.1. Case study sites

4.1.1. Weggis Slide

The largest slide in the study area, the Weggis Slide, mobilized $\sim 8.5 \times 10^6$ m^3 of sediment and is located on the northern slope of the Vitznau sub-basin (Figs. 2 and 3A). Previous studies by Siegenthaler et al. (1987), Lemcke (1992) and Schnellmann et al. (2002, 2005, 2006) have shown that this landslide is related to the 1601 A.D., $M_w \sim 6.2$ earthquake. The slide scar reaches a maximum height of 6 m and extends laterally over more than 6 km in water depths ranging from 30 to 100 m along the relatively gently dipping, 5° to 15° steep lateral slope. In Fig. 3A, the slide scar appears in approximately 35 m water depth in a zone, where the slope inclination increases downwards from <10° to ~15°. In the uppermost part of the eroded slope acoustically chaotic to transparent proximal mass-movement deposits can be identified. The observed bathymetric step in the lower part of the slope is caused by conglomerate banks of subalpine molasse rocks in the substratum. The slide scar cuts through a 4 m-thick, acoustically laminated sedimentary drape (referred to Holocene and Late Glacial deposits in Fig. 3) that overlies a thin seismostratigraphic unit characterized by a high-amplitude chaotic reflection pattern that is hardly distinguishable from the acoustic basement. This observation suggests that bedrock is covered by a few meters of glacial deposits. However, seismic penetration and resolution do not allow for exact mapping of this boundary. The absence of the entire drape clearly points towards a translational sliding mechanism with the glacial deposits acting as a base for the failure surface.

4.1.2. St. Niklausen Slide

Offshore the village of St. Niklausen in the western Chrüztrichter sub-basin (Fig. 2), stacked debris-flow deposits in the basin plain (Fig. 3B) indicate that parts of the slope have repeatedly been active in Late Glacial and Holocene times, with the youngest being the largest event that affects a total mobilized volume of $\sim 1.5 \times 10^6$ m^3. St. Niklausen Slide is smaller than the Weggis Slide described above and is of medium size compared to other Lake Lucerne subaqueous mass movements (Schnellmann et al., 2005, 2006). It was dated at 2180–2410 cal yr B.P. (Schnellmann et al., 2006) and is part of a multiple-slide event that was triggered by a major northern alpine earthquake (M_w>6.5; 2220±40 cal yr B.P.; Strasser et al., 2006). A 1.5 km-long and up to 6 m-high slide scar assigned to this 2220 cal yr B.P. slope failure event is located on a steepening-downward slope in 40–50 m water depth (Fig. 4B). Below the failure scar, a 1.6 m-thick post-landslide sedimentary drape covers the ~13° steep slope. Seismic data reveal the same acoustic characteristics as observed on the Weggis slope described above, with slightly more pronounced continuous, parallel high-amplitude reflections in the undisturbed, acoustically laminated drape upslope the failure scar (Fig. 3).

4.1.3. Chrüztrichter Slide

A third subaqueous landslide, triggered by the 1601 A.D. earthquake (Schnellmann et al., 2005), was surveyed in great detail. The relatively small Chrüztrichter Slide ($\sim 0.18 \times 10^6$ m^3 eroded volume) is located on the northeastern edge of the Chrüztrichter basin and affects an area of 0.3 km^2 from the failure scar to the toe of the deposits. The failure scar lies on a ~13° steep, northward-dipping slope of a small subaqueous mound at 30–40 m water depth. It cuts a ~6 m-thick, acoustically laminated sedimentary drape that overlies acoustic basement in the undisturbed slope environment, both upslope and lateral to the failure scar (Fig. 4).

4.2. Lithostratigraphy

The continuous glacial-to-postglacial sedimentary succession covering the undisturbed lacustrine slope at the three study sites was recovered in 6 piston cores (two at each site) immediately upslope (Weggis/St. Niklausen) or adjacent (Chrüztrichter) to the failure scar (see Figs. 2–4 for location). Figs. 5–7 show the composite plots of all data obtained at the three study sites. The sedimentary succession is very similar at all three sites and shows three distinct lithologic units composed of (from top to bottom): Unit 1 (2.5–4.9 m thick): homogenous to mottled, olive gray, silty clays with abundant organic material. The sediment is mainly of detrital origin with variable amounts of authigenically-

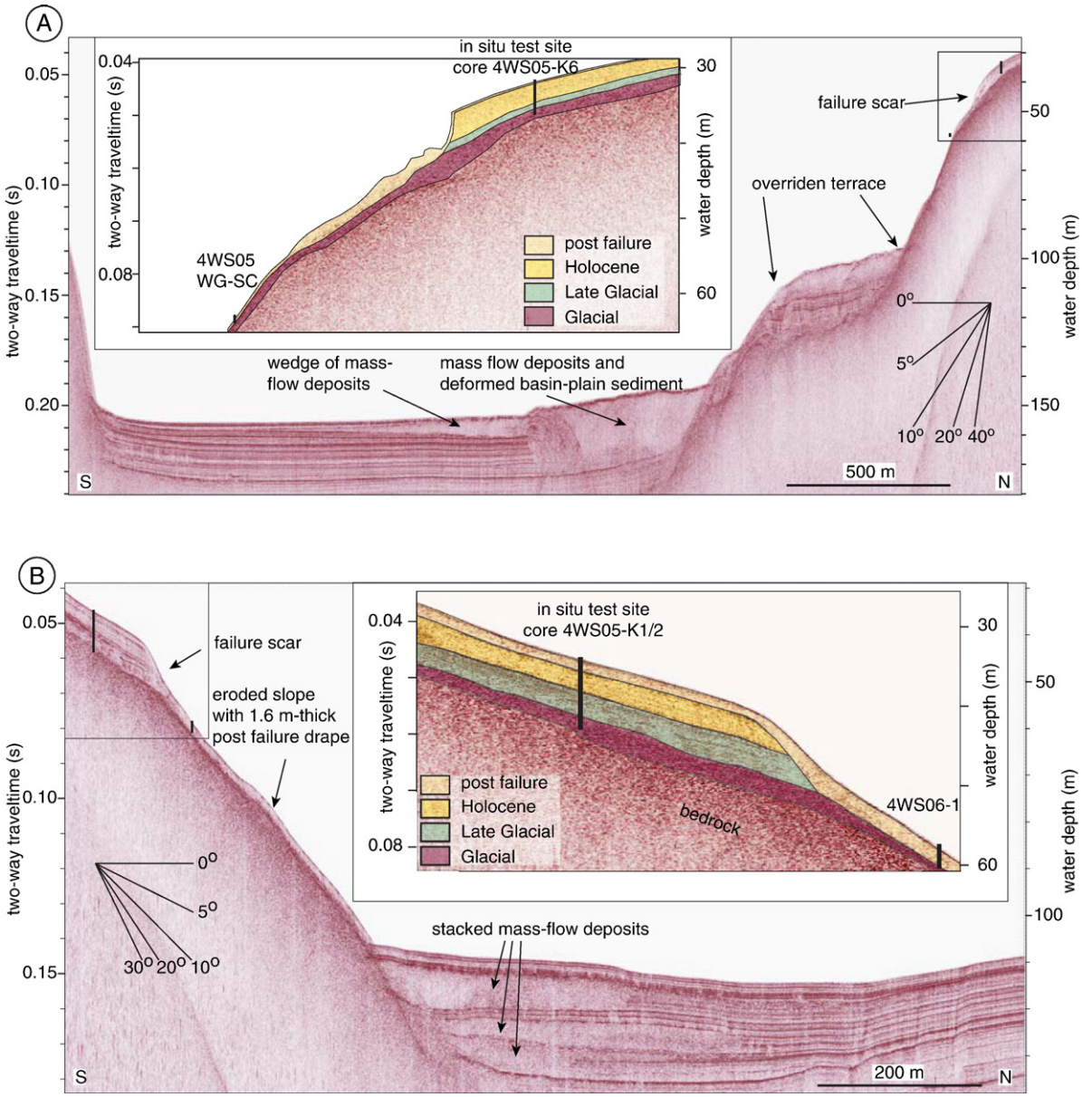

Fig. 3. 3.5 kHz seismic lines illustrating the structure of the Weggis Slide (A) and St. Niklausen Slide (B). See Fig. 2 for location of seismic lines. Inlets show enlarged details of the scars with slope model interpretations of lithological units as cored in reference cores. In the uppermost part of the eroded Weggis slope (A) the acoustically chaotic to transparent unit with an irregular upper surface is interpreted as proximal mass-movement deposit.

produced carbonates and diatoms; Unit 2 (1.2–1.6 m thick): yellowish light gray, thinly-laminated (mm to sub-mm-scale), clays and clayey silts of detrital origin (Fig. 8A); Unit 3 (1–2 m thick) tilted and deformed thinly-laminated yellowish to light gray clayey silts to silty clays with sparse (<20%) sand and medium-sized gravels up to 4 cm in diameter (Fig. 8B) floating in the fine-grained matrix. These angular, poorly sorted gravels show clear glacial striation and cover a wide range of lithologies also including crystalline basement rocks that only outcrop far south of Lake Lucerne. At the base of core 4WS05-K1 (St. Niklausen), a 15 cm-thick diamict deposit with clasts of glacial origin in a poorly sorted, clay–silt–sand matrix was recovered. Although the lowermost part of this core shows coring disturbances, this basal layer can be interpreted as a till deposit.

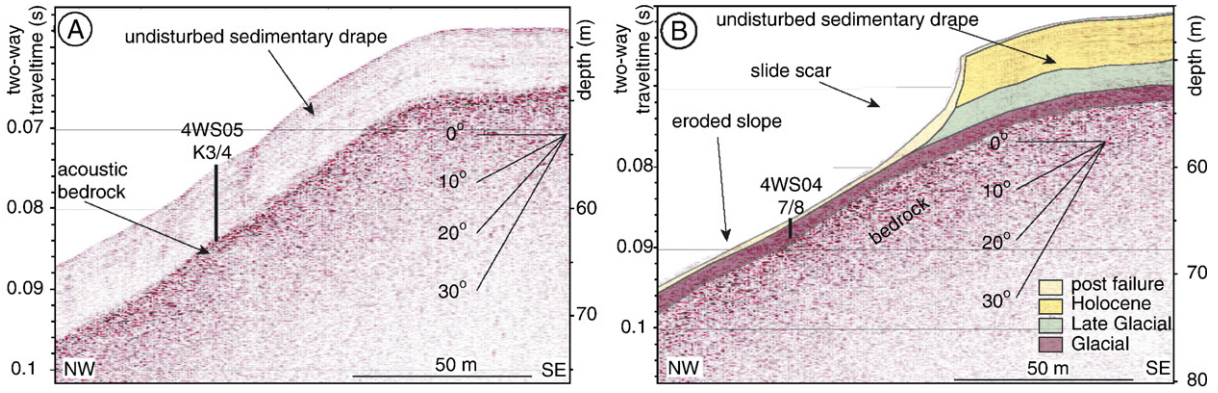

Fig. 4. Two parallel-oriented 3.5 kHz seismic lines across the sub-lacustrine slope in the northeastern edge of Chrüztrichter basin. Distance between the lines is about 80 m. For location see Fig. 2. (A) Profile shows an undisturbed slope characterized by an approximately 6 m-thick continuous sedimentary drape directly overlaying acoustic bedrock and location of cores 4WS05-K3 and K4. (B) Profile displays failure scar of Chrüztrichter Slide with slope model interpretation of lithological units as cored in reference core 4WS05-K4 and short cores 4WS04-7 and 8, which recovered the failure plane of the 1601 A.D. slope failure in core depths of 0.4 m below lake floor. Figure modified after Schnellmann et al. (2005).

Unit 3 can be assigned to the thin seismostratigraphic unit showing high-amplitude, chaotic reflection patterns as observed at the Weggis site (see Section 4.1.1) and is interpreted to represent glacially-deformed glacio-lacustrine deposits (see discussion in Section 5.1.1). Units 1 and 2 can be correlated by seismic stratigraphy, lithological facies and physical properties (mainly magnetic susceptibility and bulk density) to lithologies recovered and dated in sediment cores from the deep basin (Schnellmann et al., 2006; Thevenon et al., submitted for publication) revealing Holocene (<11 500 cal yr B.P.) and Late Glacial (>11 500 cal yr B.P.) ages, respectively. They represent the draping "slope-cover" sediment facies deposited in Lake Lucerne since the glacial retreat from the Swiss Plateau around 17 500 cal yr B.P (Lister, 1988; Wessels, 1998; see discussion in Section 5.1.2). Sedimentation rates in the Late Glacial Unit 2 are similar at the Weggis and Chrüztrichter sites (20 to 21 cm/ka) and slightly higher at the St. Niklausen site (~26 cm/ka). There, the sediments have slightly higher silt contents and few 0.5–2 cm-thick sand layers in the lower part of the postglacial section indicate higher detrital input possibly from a small local creek entering the lake nearby. In contrast, sedimentation rates for the Holocene Unit 1 differ significantly from site to site. At the Weggis site, they are in the same order as during Late Glacial times (~22 cm/ka), while they are clearly higher along the submerged slope offshore St. Niklausen (~36 cm/ka) and reach maximal values at the Chrüztrichter site (42 cm/ka). The difference in sedimentation rate may be caused by small local creeks, currents (Aeschbach-Hertig, 1994) and different amounts of biogenic sedimentation that favors deposition along the St. Niklausen and Chrüztrichter slope.

4.3. Physical properties

Physical property data from all three sites reveal significant contrasts in most measured parameters between the postglacial (Units 1 and 2) and the glacio-lacustrine deposits (Unit 3; Figs. 5–7). Generally, the Holocene section is characterized by downward increasing values of bulk density (ρ_{bulk}) with depth, whereas natural water content and Atterberg limits decrease gradually downsection. Only solid grain densities are more or less constant throughout the section with values of ~2.75 g/cm^3 and ~2.8 g/cm^3 in the Holocene deposits and in the Glacial to Late Glacial material, respectively. At the Weggis site, absolute ρ_{bulk} values increase stepwise at lithological boundaries from 1.3–1.4 g/cm^3 in Unit 1 to 1.45–1.55 g/cm^3 in Unit 2, whereas at the two other sites, ρ_{bulk} values more gradually increase from ~1.3 g/cm^3 in the middle part of the Holocene section to ~1.55 g/cm^3 in the Late Glacial deposits. The boundary between the postglacial and the glacial deposits is characterized by a dramatic increase in ρ_{bulk} of ~0.3 g/cm^3 at Weggis and Chrüztrichter sites. This boundary is further characterized by a significant change in the liquidity index, because natural water contents (w) in the postglacial sediments (decreasing from ~150–175% of dry weight in the uppermost part to ~60–75% in the laminated Late Glacial clays) are higher than the liquid limits (w_L) of these sediments, whereas w values (~40–50%) plot below the respective w_L-values in the glacio-lacustrine deposits of Unit 3. However, at the St. Niklausen site the contrast in physical properties between

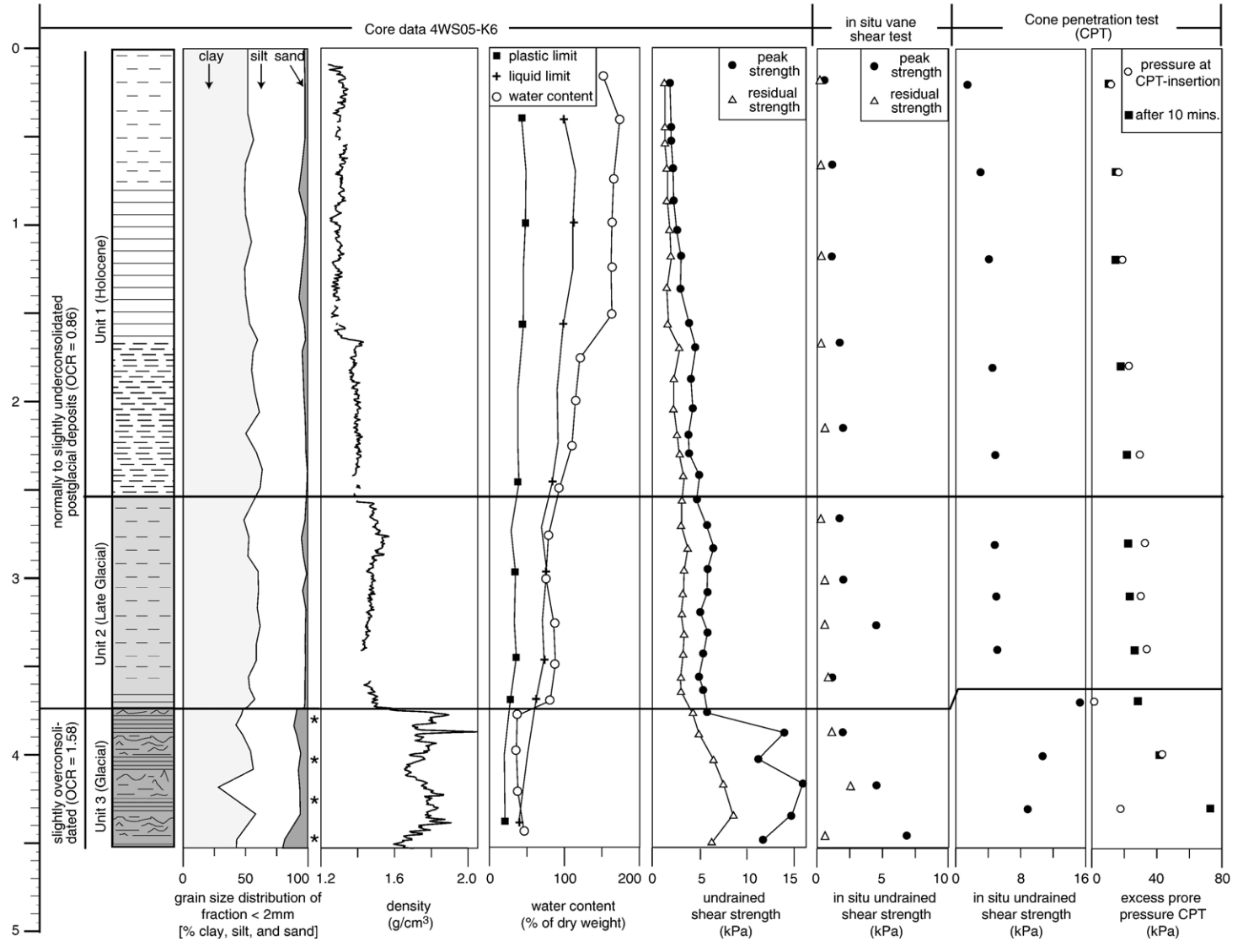

Fig. 5. Data obtained from core 4WS05-K6 and from in situ tests summarizing sedimentological and geotechnical characteristics of the undisturbed continuous glacial-to-postglacial sedimentary succession covering the sub-lacustrine slope offshore Weggis. The site is located immediately upslope the failure scar (see Figs. 2 and 3A for location). Asterisks indicate the presence of material with grain size >2 mm (that are not considered in this plot).

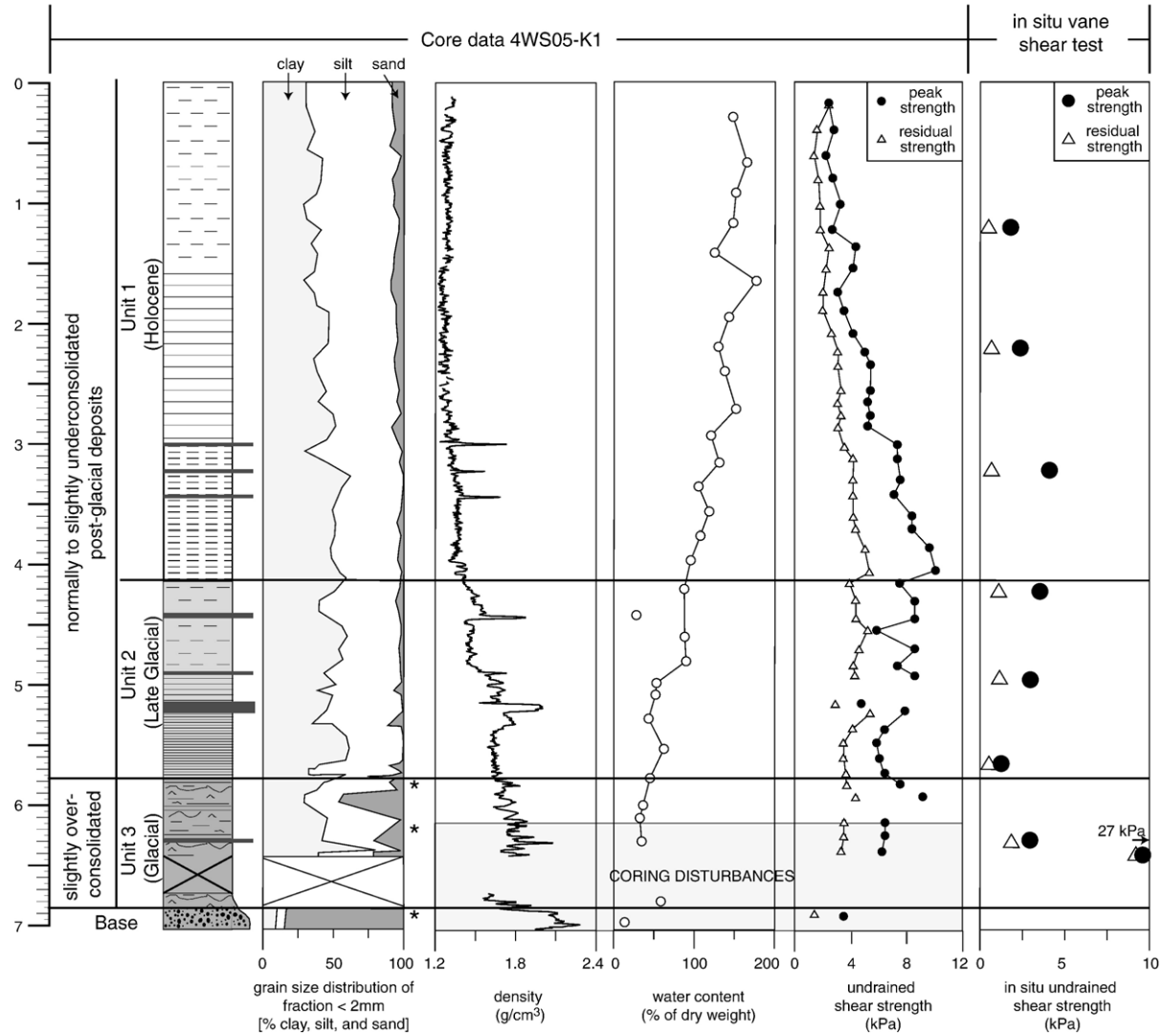

Fig. 6. Data obtained from core 4WS05-K1 and from in situ tests summarizing sedimentological and geotechnical characteristics of the undisturbed continuous glacial-to-postglacial sedimentary succession covering the sub-lacustrine slope offshore St. Niklausen. The site is located immediately upslope the failure scar (see Figs. 2 and 3B for location). Asterisks indicate the presence of material with grain size >2 mm (that are not considered in this plot).

the postglacial sediments and glacial deposits is less pronounced than at the other sites (Fig. 6). This is most likely caused by coring disturbances in the lowermost part of core 4WS05-K1.

At the Weggis site, two samples from immediately above and below the characteristic boundary between Units 2 and 3 were examined with one dimensional consolidation tests (oedometer) to determine the consolidation history and relative permeability of the material. Results reveal that the laminated Late Glacial clays are slightly underconsolidated (OCR = 0.86) whereas the glacio-lacustrine deposits of Unit 3 are overconsolidated (OCR = 1.58). Both sediment types show low permeability, with the plastic glacial material from Unit 3 being less permeable (hydraulic conductivity (K) = 5.35×10^{-10} m/s) than the postglacial sample ($K = 5.32 \times 10^{-9}$ m/s) (for details see Stegmann et al., in press).

4.4. Shear strength

Undrained peak (c_u) and residual shear strengths slightly vary with respect to the three different test methods utilized, but all three approaches reveal the

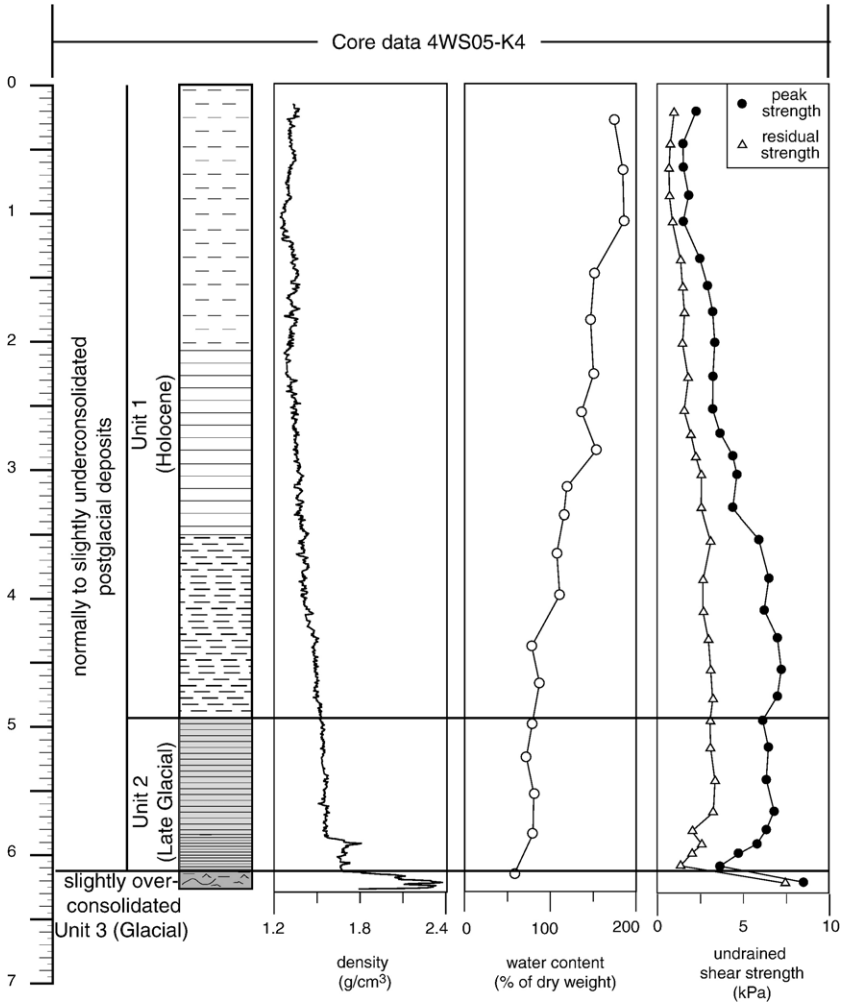

Fig. 7. Data obtained form core 4WS05-K4 summarizing sedimentological and geotechnical characteristics of the undisturbed continuous glacial-to-postglacial sedimentary succession covering the sub-lacustrine slope at the study site in the source area of the Chrüztrichter Slide. The site is located adjacent to the failure scar (see Figs. 2 and 4 for location).

same relative trend (Figs. 5–7): The Holocene Unit 1 is characterized by linearly increasing c_u values with depth, whereas values in the upper part of the Late Glacial Unit 2 are constant and even show a clear downward decrease immediately above the contact with the glacial deposits that again show significantly higher strength values (well pronounced at St. Niklausen and Chrüztrichter sites; Figs. 6 and 7).

Measured $c_{u\ in\ situ}$ values from in situ vane shear tests generally show slightly lower values than those from in situ CPT and laboratory test. This result is interpreted to be caused by disturbances to the material during probe insertion and small waves during the vane shear testing, resulting in slight underestimates of $c_{u\ in\ situ}$ (see Section 3.3). At the Weggis site, $c_{u\ in\ situ}$ values derived from CPT testing and c_u values obtained from laboratory tests correlate well and reveal similar values that increase within the upper 2.5 m (Unit 1) to ~5 kPa. At the St. Niklausen and Chrüztrichter sites, highest laboratory-derived c_u values at the base of the Holocene Unit 1 reach 9 and 7.5 kPa, respectively. In the laminated Late Glacial clays of Unit 2, c_u values vary between 5–8 kPa (laboratory and in situ CPT-test) and 2–5 kPa (in situ vane shear test) but indicate more or less constant strength characteristics in the upper part and a clearly downwards decreasing trend in the lowermost part of the cores. The glacio-lacustrine sediments of Unit 3 show significantly higher strength values, but absolute values derived from the different methods scatter between 3 and 27 kPa. The fact that Unit 3 shows

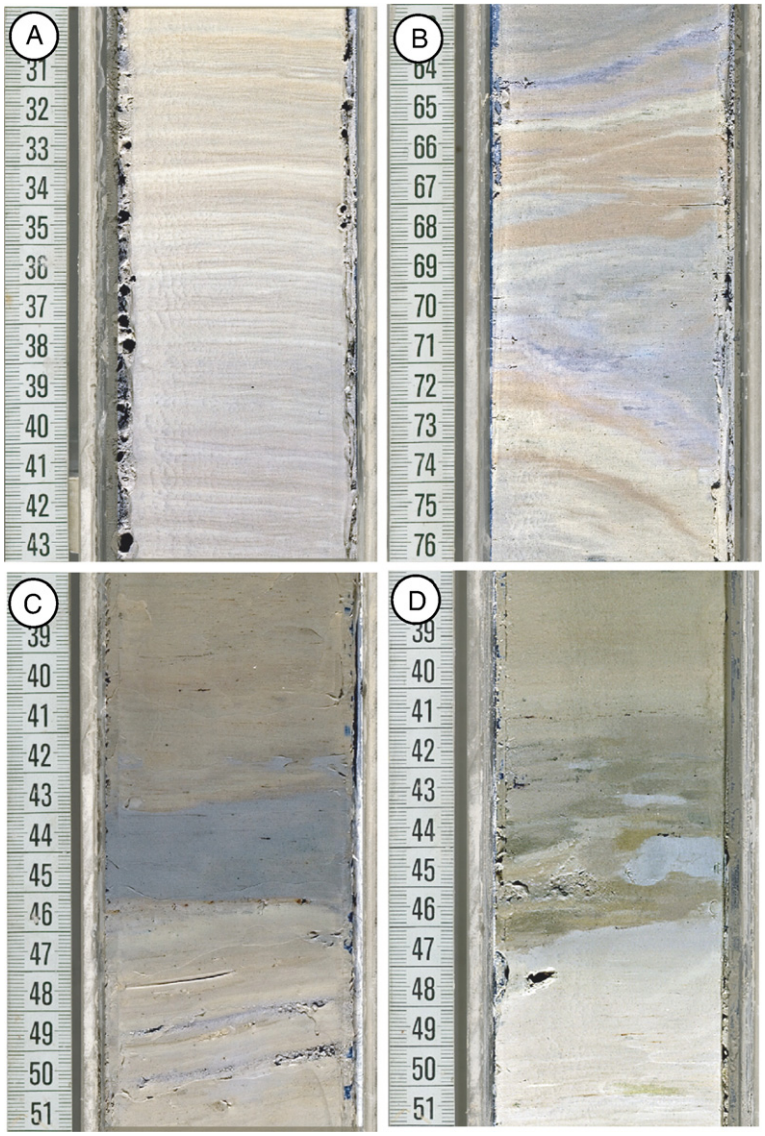

Fig. 8. Core photographs showing: A) thinly-laminated Late Glacial clays (core 4WS05-K6); B) glacially-deformed overconsolidated glacial-lacustrine deposits (core 4WS05-K6); C) 2 cm-thick, grey homogenous silty clay layer between 44 and 46 cm of core 4WS05-WG/SC assigned to the Weggis Slide overlying tilted glacio-lacustrine deposits; and D) sharp and erosive boundary at 46 cm of core 4WS04-7 (i.e. failure plane of Chrüztrichter Slide) between glacially-deformed glacio-lacustrine deposits and post-landslide deposits. Note reworked glacial mud clasts (at 45 cm) at the base of the overlying post-landslide deposits.

some heterogeneity with slightly higher sand content (up to 20%) and presence of gravels (see Section 4.2), vane shear tests might not be perfectly applicable and partly account for the scatter. However, as the bulk sediment in this lower section consists mainly of silty clay with a relative low permeability, undrained loading conditions predominate (Lambe and Whitman, 1979). Thus, the measured undrained strength values are interpreted to adequately represent the strength characteristics in this unit.

4.5. In situ pore pressure (Weggis site)

At the Weggis site, in situ formation pore pressure ($u_{\text{in situ}}$) was estimated after 10 min of monitoring the pressure evolution after CPT insertion at different target depths. Fig. 5 shows measured excess pore pressure values (i.e. absolute measured pressure minus hydrostatic pressure) at CPT insertion and after 10 min. All tests conducted in the postglacial section reveal dissipation curves with a pore pressure spike upon

impact of the probe, followed by a non-linear asymptotic decay. Although ambient excess formation pore pressure cannot be extrapolated from only 10 min of monitoring, the characteristic exponential decay of the dissipation curves points toward equilibrium values slightly above hydrostatic. In the glacio-lacustrine sediments of Unit 3, however, the monitored pore pressure after insertion shows the opposite trend. Insertion pressures are relatively low compared to the postglacial sediments, possibly due to suction and fluid displacement at the tip during insertion or due to a dilatant material response. With time, however, pressure increases significantly. This observation is interpreted to result from considerably elevated formation pore pressure in Unit 3. One test carried out for about 45 min attested that a plateau in pore pressure rise is reached after approximately 25 min.

4.6. Failure plane characteristics

Short gravity cores from the slide-eroded slopes at all three sites recovered tilted and deformed glacio-lacustrine deposits (Unit 3) in 0.36, 0.4 and 1.6 m core depth at the Weggis, Chrüztrichter and St. Niklausen sites, respectively. The upper boundary of the glacial deposits in all cores is sharp and erosive. These boundaries are interpreted as the failure surfaces of the 1601 A.D. and 2220 cal yr B.P earthquake-triggered landslides (Weggis/Chrüztrichter and St. Niklausen Slides, respectively). At the two 1601 A.D. landslide sites, the thickness of overlying post-landslide deposits (Unit 1) reveals sedimentation rates for the last 400 yr of ~1 mm/a, which is consistent with estimated recent sedimentation rates by Lemcke (1992). At St. Niklausen, the 1.6 m thick deposition of post-landslide sedimentary drape on the eroded slope reveals mean sedimentation rates over the last 2220 yr in the order of ~0.75 mm/a. At the Weggis site, a gray, 2 cm-thick, homogenous silty clay layer overlying the failure surface can be related to the Weggis Slide (Fig. 8C). Additionally, reworked glacial mud clasts recovered at the base of post-landslide deposits at the Chrüztrichter and St. Niklausen sites (Fig. 8D) clearly pinpoint the failure surfaces to be related to the glacio-lacustrine Unit 3. However, as observed in the seismic data, there are no evidences for significant erosion of Unit 3 during translational sliding (Figs. 3 and 4). Therefore, combined geophysical subsurface and core data suggests the failure to be located immediately at the top of the glacial Unit 3.

5. Discussion

Results from our study consistently imply that, regardless of regional variations between the sub-basins, initiation and evolution of earthquake-triggered lateral subaqueous slope failures occurred along glide planes that developed at the lithological boundary between overconsolidated, overpressured glacio-lacustrine deposits (Unit 3) and weak, slightly underconsolidated laminated Late Glacial clays (Unit 2). Similarly, it has been reported from other studies in perialpine, fjord-type lakes and fjords that slides also mobilized the slope-covering drape down to glacial deposits comparable to those described here (e.g. *Horgen Slide* and *Oberrieden Slide* in Lake Zurich, Switzerland (Kelts, 1978; Strasser 2006, unpublished data); *Pointe-Du-Fort Slide* in Saguenay Fjord, Canada (Locat et al., 2003); submarine slides in Karmsundet and Skudenesfjorden, Norway (Boe et al., 2000)). It is thus interpreted that the glacial-to-postglacial evolution in sedimentation processes along the lateral slopes in similar settings as Lake Lucerne results in characteristic physical and geotechnical properties that eventually control the stability conditions and that in turn favor subaqueous slope failure initiation at systematic stratigraphic levels.

In the following section, a conceptual slope-sedimentation model since the last glaciation is presented (Fig. 9), and its control on the evolution of the physical properties is discussed. In the subsequent section, the measured geotechnical parameters are implemented into limit equilibrium models in order to quantitatively assess the slope stability condition of the submerged slopes at the time of failure.

5.1. Sedimentation model and its influence on the geotechnical properties

5.1.1. Glacial

The sedimentary facies of the tilted and deformed laminated clayey silts with sparse sand and glacially striated, allochtonous gravels (Unit 3) clearly point towards deposition in a glacio-lacustrine environment and subsequent glacial deformation by ice-grounding and/or ploughing. The fact that the material experienced higher pre-consolidation pressure than the effective overburden stress today (OCR > 1) can in this context be interpreted to result from glacial compaction under the additional weight of ice mass acting on the material. Additionally, long-term postglacial secondary compression within the compressible glacio-lacustrine clays and silts (Terzaghi et al., 1996) may also partly explain the observed formation-wide overconsolidation. Other processes that would lead to overconsolidation, such as erosion of previously overlying material or diagenetic cementation, are ruled out, because evidence favoring these processes was neither observed in the seismic data

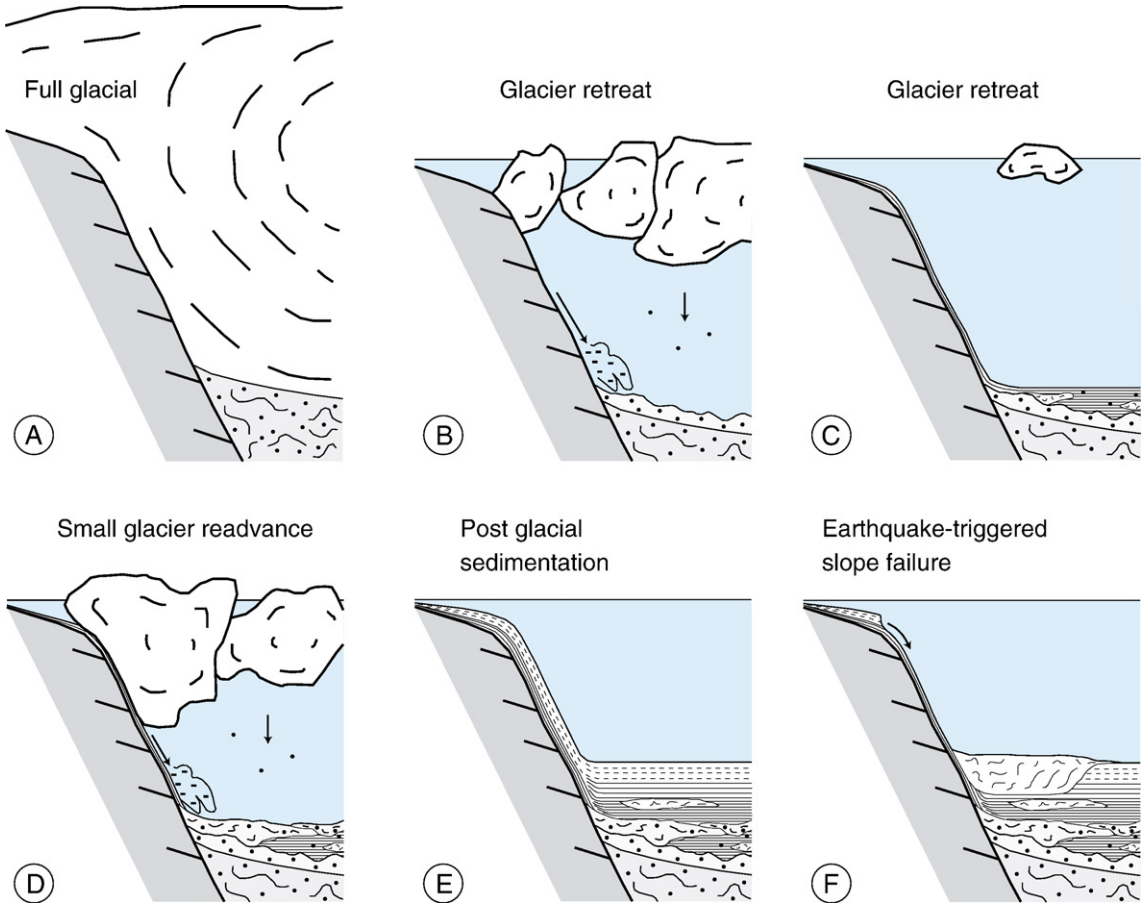

Fig. 9. Conceptual glacial-to-postglacial sedimentation model along lateral non-deltaic slopes in perialpine fjord-type lakes. Schemes (not to scale) are perpendicular to the basin axis and show schematically the depositional and post-depositional processes acting on the submerged slope: (A) Last Glacial Maximum: the basin is fully occupied by the glacier. Glacial bedrock erosion rather than sedimentation occurs along the slopes; (B) Glacial decay results in the formation of a sub-glacial lake (see Section 5.1.1). Glacio-lacustrine deposition occurs focused in the deep basin; along the lateral slope, little sedimentation, erosion, creeping and slumping occurs. (C) Further rapid disintegration of remaining glacial ice back to shallower up-valley parts results in a periglacial setting where a fine veneer of fine-grained sediments also is deposited along the lateral slopes settling out from meltwater plumes. (D) Relatively short-lived periods of colder climate conditions result in minor glacial readvances, during which ploughing and grounding of icebergs along the slope leads to deformation and compaction of the glacio-lacustrine sediment. (E) After the final glacier retreat suspension settling from meltwater plumes and settling from flood-induced over and interflows mixed with authigenic carbonate production occurs during the Late Glacial and Holocene, respectively. Continuous sedimentation "charges" the slopes until external trigger mechanism triggers slope failures. (F) Post-failure situation.

nor in cored material. Glacial compaction and secondary compression also results in reduction of permeability. Therefore, the observed pore fluid overpressures in Unit 3 are interpreted to be a result of the limited drainage capacity in these relative low permeable deposits. The process of overpressuring, however, remains unknown. One possibility is that elevated pore pressures were initially induced during partially undrained glacial compaction and sustained thereafter, although one would rather expect the formation pore pressure to stabilize over such a long time period. Alternatively, and more likely, there could be an influence from a recent local groundwater flow sustaining a positive lateral flux that results in higher pore pressures than expected under hydrostatic conditions.

Because the observed glacial overconsolidation of the deposits is relatively low (OCR = 1.58), we exclude that glacial compaction took place during times when the glacier fully occupied the deep basins and the study sites were covered by ~800 m of ice (Florineth and Schluchter, 1998). Therefore, the glacio-lacustrine deposits have to be younger than the Last Glacial Maximum (~24–19 ka B.P; Ivy Ochs et al., 2004). Generally, deglaciation of glacially over-deepened

basins such as Lake Lucerne occurred by stagnation-zone retreat rather than by the retreat of an active glacier front (Lister et al., 1984). Deposition of glacio-lacustrine sediments first takes place in the deep basin of a sub-glacial lake that formed once the buoyancy of the ice body exceeds its weight and the glacier floats up. Further ablation, water contact melting, and calving lead to rapid disintegration of remaining glacial ice back to shallower up-valley parts (e.g. Haeberli and Schlüchter, 1987). Most of the sediment is deposited in the topographic depressions but a thin veneer of fine-grained glacio-lacustrine sediments is also deposited along the lateral slopes settling out of meltwater plumes containing suspended glacial mud (e.g. Mackiewicz et al., 1984; Blass et al., 2003; Anselmetti et al., in press; Fig. 9C). Sand and gravel clasts occasionally are deposited as ice-rafted debris. In this highly dynamic periglacial setting, relatively short-lived periods of colder climate conditions result in minor glacial readvances with higher intensities of ice-calving, during which ploughing and grounding of icebergs along the lateral slopes result in deformation and compaction of the glacio-lacustrine sediment (Fig. 9D).

5.1.2. Post Glacial

After the final glacier retreat (~17 500 cal yr B.P.; Lister, 1988; Wessels, 1998), most of postglacial sedimentation occurs on deltas and is focused in the topographic depressions of the deep basins through underflow processes. However, suspension settling from meltwater plumes that uniformly distribute the fine fraction of the suspended glacial mud over the lake basin also drapes the submerged lateral slopes (Fig. 9C). Cyclic (e.g. seasonal) fluctuations in meltwater discharge result in thinly-laminated and fine-grained draping slope deposits as recovered in the lower part of Unit 2 (Fig. 8A), which potentially could represent proglacial clastic varves (Mackiewicz et al., 1984; Blass et al., 2003; Anselmetti et al., in press). With further glacial retreat into the alpine valley during Late Glacial times, the influence of glacial meltwater plumes on the lacustrine sedimentation is continuously diminished and suspended material entering the lake as under-, inter- and overflows after high precipitation and flood events continuously dilutes the rhythmically laminated Late Glacial clays. With climate amelioration at the Late Glacial to Holocene transition around 11 500 cal yr B.P., sedimentation along the slope is increasingly influenced by both authigenic carbonate and biogenic production as well as detrital input from small local rivers during high discharge events (Sturm and Matter, 1978). This observed change in the sedimentation processes along the lateral slopes reflects the general Late Glacial to Holocene shift in the sedimentary system also recorded in many other perialpine lakes (e.g. Van Rensbergen et al., 1999; Eyles et al., 2000; Beck et al., 2001) and fjords (e.g. Evans et al., 2002; Lysa et al., 2004). It further explains the increased sedimentation rates along the lateral slopes during the Holocene compared to Late Glacial times, as estimated from the core data (see Section 4.2).

The distinct differences in Late Glacial and Holocene sedimentation mechanisms also influence the strength characteristics of the slope-covering material. In the Holocene Unit 1 gradients of undrained shear strength with depth (∇c_u) are constant in the order of ~1.8 kPa/m (Weggis ~1.75 kPa/m, St. Niklausen ~2.0 kPa/m, Chrüztrichter 1.75 kPa/m). Similar Holocene $-\nabla c_u$ values also have been reported from in situ testing results in other Swiss lakes (Gyger et al., 1976). Sediment strength thus correlates with effective stress (ratio c_u/σ'_v ~0.2–0.4) and the characteristic profiles suggest a continuous self weight consolidation associated with a relatively continuous sedimentation rate. In contrast, c_u values in the Late Glacial clays (Unit 2) are constant in the upper part and even reveal negative c_u-gradients at their base, where the lamination of proglacial cyclic plume deposits is well pronounced. This observation suggests a connection between the laminated clays and their unfavorable stability conditions. Indeed, geotechnical investigations of similar Late Glacial varve-deposits in Switzerland and Canada show significant influences of the clay lamination and microstructure on strength characteristics and mechanical behavior (e.g. Quigley and Ogunbadejo, 1972; Plötze et al., 2003). Additionally, the postglacial deposits are characterized by slight formation overpressures, which is interpreted to be related to the relatively high sedimentation rates (20–40 cm/ka) and incomplete drainage of the low permeable sediments. As a consequence, the normal consolidation phenomenon is retarded and the sediment is in an underconsolidated state (Sultan et al., 2004), as measured by consolidation tests (OCR = 0.86).

In summary, the depositional and consolidation mechanism of sediments covering the submerged lateral slope of Lake Lucerne created particular sedimentological and geotechnical slope characteristics that control the stability condition and that predefine the eventual failure location. With an external trigger mechanism (i.e. strong seismic shaking) these lithologically inherited conditions result in subaqueous slope failure initiation along the boundary between overconsolidated glacio-lacustrine deposits with overpressured formation pore

pressures (Unit 3) and slightly underconsolidated laminated Late Glacial clays (Unit 2) characterized by low shear strength values at their base. Based on the principle of effective stress, Stegmann et al. (in press) show in detail that, as a result of co-seismic stress fluctuations and stress-transfer upward to the base of the weaker unit, pore pressure exceeds lithostatic load and initiates sliding along a failure plane developing at the boundary between Units 2 and 3.

5.2. Limit equilibrium slope stability analysis

In order to reconstruct slope failure conditions at the study sites and to quantify seismic ground accelerations affecting the slopes at the time of failure, the obtained data were implemented into a limit equilibrium slope stability model that serves to back-analyze the slope failures triggered by the historic 1601 A.D. and the prehistoric 2220 cal yr B.P earthquakes. At both Weggis and St. Niklausen sites, the pre-failure slope geometry was reconstructed as a 3-layer model (Units 1–3) assuming constant sediment thicknesses as recovered in the reference cores immediately upslope of the failure scars and subtracting the uppermost post-landslide deposits as recovered in short cores along the eroded slopes. This assumption is justified by seismic data that show constant sediment thicknesses in undisturbed sections draping the slope adjacent to the slide. The lower model boundary was chosen to be 1 m below the boundary between Units 2 and 3, modeling the thickness of the overconsolidated glacial Unit 3 as indicated in the seismic data (see Section 4.1). Mean ρ_{bulk}, c_u at the layer top and ∇c_u were assigned to each layer according to results from core analysis and in situ testing (Table 1). Based on the observation in the geophysical subsurface data and on the results from in situ and cores analysis, the glide plane along which translational sliding occurred, is interpreted to correspond to the lithological boundary between Unit 2 and Unit 3 (see Sections 4.6 and 5.1). Therefore, a failure plane at the boundary between these to units was predefined in the slope stability analysis.

For all analysis it was assumed that the sediment is subjected to undrained loading conditions because cyclic loading during earthquake shaking is rapid enough that excess pore pressure does not have time to dissipate through the fine-grained medium. The slightly higher sand content in Unit 3 potentially could indicate that loading conditions in the lowermost unit might not fully be undrained. Also, liquefaction induced by pore pressure increase during seismic shaking cannot completely be excluded as potential failure initiation mechanism. However, given the relatively low permeability and predominant fine-grained character of the glacial deposits, undrained loading is interpreted to be the predominant mechanism at the critical depth where failure occurs. Liquefaction as potential failure initiation processes is interpreted to by unlikely because estimations of the susceptibility for liquefaction based on a rough criterion proposed by Andrews and Martin (2000) reveal no critical conditions (i.e. measured clay contents and liquid limits at critical depth in all cores are much higher than critical values of 10% and 32%, respectively). Additional uncertainties in our slope stability analysis arise from the fact that the used pseudostatic modeling approach does not consider the dynamic behavior of the sediment and therefore does not account for potential failure mechanism in addition to the load generated by horizontal seismic acceleration (e.g. degradation of soft clays, accumulation of plastic strains and shear-induced excess pore water pressure with increasing number of cycles (Sultan et al., 2004; Biscontin et al., 2004)). Future investigations on the dynamic behavior of the material under cyclic loading as well as detailed clay mineralogy analysis are required in

Table 1
Geotechnical parameters used for deterministic limit equilibrium back-analysis

	Layer thickness d	Unit weight γ	Undrained shear strength at the top of layer c_u	Undrained shear strength gradient with depth ∇c_u
	(m)	(kN m^{-3})	(kPa)	(kPa m^{-1})
Weggis site at 1601 A.D.				
Layer 1 (Holocene)	2.5	13.25	1	1.75
Layer 2 (Late Glacial)	1.25	14.72	5.4	0
Layer 3 (Glacial)	1	17.7	Varying values	5
St. Niklausen site at 2220 cal yr B.P.				
Layer 1 (Holocene)	2.7	12.8	1	2
Layer 2 (Late Glacial)	1.6	14.72	7.1	0
Layer 3 (Glacial)	1	17.7	Varying values	5

order to better constrain these uncertainties. Therefore, our pseudostatic limit equilibrium model used here only represents a first order estimation of quantifying seismic ground accelerations that affected the Lake Lucerne slopes during past earthquakes.

Sensitivity analysis of the model used in this study revealed that the impact of c_u at the depth of failure and the horizontal acceleration a_H is several-fold higher in comparison with the other parameters for the chosen slope geometry and failure plane location. Absolute c_u values slightly vary with respect to the three different measurement methods and therefore add uncertainties in the back-calculated critical pseudostatic seismic ground acceleration. The back-analysis was therefore carried out with varying values of c_u at the top of Unit 3 and results are presented as contour plots showing the factor of safety (FS) as a function of both c_u at the depth of failure and a_H (Fig. 10).

For the Weggis site, measured c_u values at the top of Unit 3 vary between 3 and 6 kPa as measured with the different independent methods, whereas they are slightly higher at the St. Niklausen site. Results of deterministic stability analysis using these c_u ranges reveal that both slopes are stable under static loading condition (i.e. $a_H=0$) with FS ranging between 1.1 to 1.7 and 1.3 to >2, respectively. As discussed above, the lower values estimated from in situ vane shear tests most probably underestimate the actual strength conditions, so that realistic $c_{u\ in\ situ}$ should be ~5 kPa at the Weggis and ~6 kPa at St. Niklausen site, as inferred from in situ CPT tests. Using these values for the model input reveal static FS between ~1.5 and 2 at Weggis and St. Niklausen, respectively. To trigger slope failure at the Weggis site, an additional pseudostatic seismic acceleration between 0.01 and 0.06 g (~0.04 g, if applying the estimated probable $c_{u\ in\ situ}$ value of ~5 kPa) is required, whereas the slope at St. Niklausen remains stable up to critical a_H values between 0.03 and 0.08 g (~0.07 g, if applying the estimated probable $c_{u\ in\ situ}$ value of ~6 kPa) (Fig. 11).

Leynaud et al. (2004) suggested that the pseudostatic horizontal seismic acceleration only represents about 50% of the effective earthquake peak ground acceleration (PGA). Results from slope stability back-calculations thus imply minimal PGA's of about 0.08 g (range of uncertainty ~0.02 to 0.12 g) and ~0.14 g (range of uncertainty ~0.06 to 0.16 g) during the 1601 A.D. and the 2220 cal yr B.P. earthquake, respectively. The result for the 1601 A.D. event from the Weggis site lies in the range of calculated values for PGA's deduced from predictive ground motion models for Central Switzerland (Bay et al., 2005), assuming a M_w 6.2 earthquake and an epicentral distance of 12 km (Fig. 1). The estimated PGA value for the prehistoric 2220 cal yr B.P earthquake in the order of 0.14 g, however, is slightly higher than the expected ground motion induced by low frequency (1 Hz) seismic

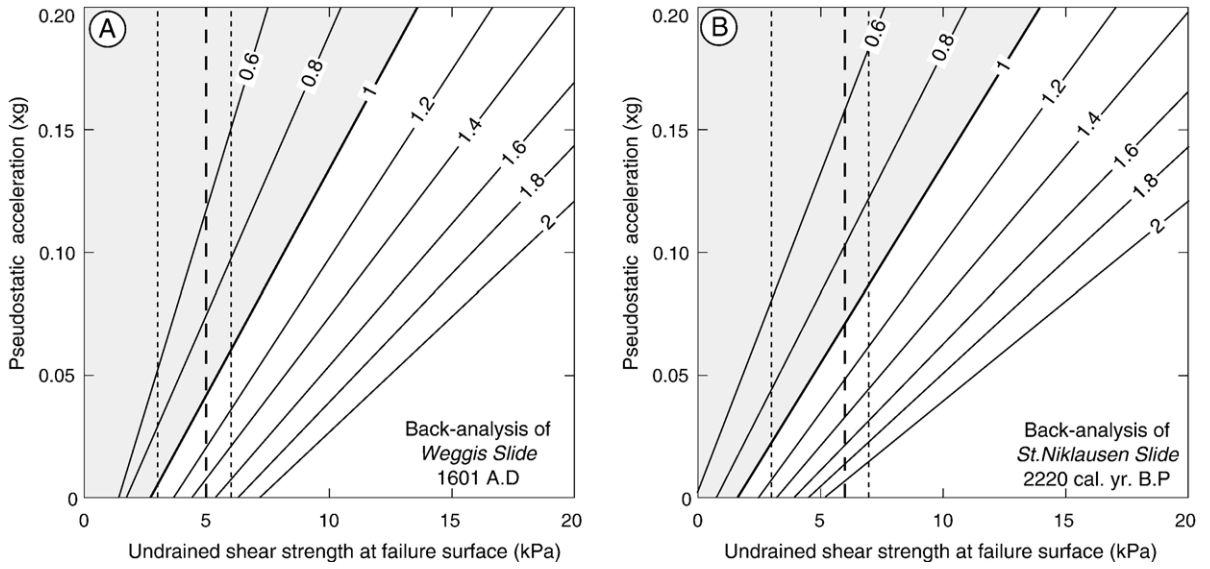

Fig. 10. Results of deterministic limit equilibrium slope stability back-analysis of Weggis (A) and St. Niklausen (B) Slides during the 1601 A.D. M_w ~6.2 earthquake and the 2220 cal yr B.P. earthquake (M_w>6.5), respectively. Contour plots show factor of safety (FS) as a function of the undrained shear strength at the failure surface and the pseudostatic acceleration (fraction of gravitational acceleration g). The gray shaded areas indicate solutions leading to instable conditions (FS<1). The range and reliable in situ values of measured undrained shear strength at the two study sites is shown as a fine dotted and bold dashed line, respectively. See Table 1 for model input data.

Table 2
Geotechnical material statistics used for probabilistic limit equilibrium slope stability analysis

	d (m)	γ (kN m^{-3})				c_u (kPa)				∇c_u (kPa m^{-1})			
		Mean	S.D.	Relative min	Relative max	Mean	S.D.	Relative min	Relative max	Mean	S.D.	Relative min	Relative max
Weggis site at 2220 cal yr B.P.													
Layer 1	1.5	13.3	0.3	0.5	0.5	1	0.5	0.5	0.5	1.75	0.5	0.75	0.5
Layer 2	1.25	14.7	0.5	0.5	0.5	5.4	3	3	3	–	–	–	
Layer 3	1	17.7	1	1	3	5.4	2.5	2.4	2	5	2	3	5
Chrüztrichter site at 2220 cal yr B.P.													
Layer 1	3.4	13.3	0.3	0.5	0.2	1	0.5	0.5	0.5	1.75	0.5	0.75	0.5
Layer 2	1.2	14.7	0.5	0.5	0.5	7.5	3	5	0.5	−2	0	1	2
Layer 3	1	20.6	1	3	1.5	8.5	2.5	4.5	2	5	2	3	3

Pseudostatic acceleration k_H during 2220 cal yr B.P earthquake ($\times g$)	Mean	S.D.	Relative min	Relative max
	0.07	0.03	0.012	0.023

waves with a return period of 2500 yr as estimated by probabilistic earthquake hazard assessment for the Lake Lucerne area (Giardini et al., 2004).

Although one would need to consider site effects that might amplify or attenuate seismic shaking and the fact that the accuracy of the used pseudostatic approach is governed by the simplification, with which the pseudostatic inertial forces represent the complex dynamic inertial forces during earthquake shaking (Kramer, 1996), the results from slope stability back-analysis suggest that during the prehistoric 2220 cal yr B.P earthquake that triggered the St. Niklausen Slide the Lake Lucerne area experienced significantly higher ground motions than during the historic 1601 A.D. $M_w \sim 6.2$ earthquake. This interpretation is supported by the fact that the 2220 cal yr BP earthquake also triggered subaqueous landslides in Lake Zurich at a distance of 40 km from Lake Lucerne, requiring a significantly larger magnitude ($M_w > 6.5$) than the historic 1601 A.D. earthquake (Strasser et al., 2006). However, the interpretation of higher ground motions during the 2220 cal yr B.P. event seems to contradict the observation that the Weggis and Chrüztrichter slopes remained stable during this stronger prehistoric event.

In order to investigate this apparent contradiction, the Weggis and Chrüztrichter slope stability conditions at 2220 cal yr B.P. were analyzed with a probabilistic limit equilibrium approach using the calculated critical horizontal seismic accelerations by the back-analysis described above (Table 2 summarizes the input parameters used). Both scenarios reveal mean FS values >1 (1.03 and 1.14) and failure probability of <50% (45.6 % and 43.7 %) for both the Weggis and Chrüztrichter slopes, respectively. Both slopes were relatively close to failure, but obviously remained stable during the 2220 cal yr B.P. event. These results indicate that the "charging" state of a submerged slope is a function of the sedimentation rate during the Holocene (i.e. the only parameter changing significantly from site to site), that controls the static weight of the slope-covering drape. Similar conclusions were drawn based on a significant increase in the frequency of lateral mass-movement deposits identified during Holocene times in other lakes (e.g. Waldmann et al., submitted for publication).

These observations further imply that ongoing sedimentation along the submerged slopes will continuously load the slopes so that the susceptibility for slope failure will increase in the future. As an end member scenario we investigated how long it would take to charge the Weggis slope (assuming constant sedimentation rates), so that the sediments acting on the critical surface would become unstable under static loading conditions. Solving the infinite slope equation (Morgenstern, 1967) for critical sediment thickness to initiate failure reveals as a first order assumption that the slopes only will become statically unstable in ~24 500 yr (input parameters: mean values for c_u, μ' and α as observed in the data described above). This is one order of magnitude longer than the time that separated the last two major earthquakes around Lake Lucerne implying that the occurrence of seismic events acts as main control on landslide triggering. Local differences in site-specific stability conditions, however, are governed by regional variations in sediment supply so that slope stability conditions may change locally over relative short geological time scales.

6. Summary and conclusions

This study presents the results from three comprehensive case studies of seismically-triggered, lateral non-deltaic subaqueous slope failures in perialpine, fjord-type

Lake Lucerne (Central Switzerland). The combined sedimentological, geophysical and in situ geotechnical approach provides a better understanding of the influence of the glacial-to-postglacial evolution in sedimentation processes along the investigated lateral slopes and their impact on the characteristic physical and geotechnical properties of the slope-covering sediments that control the stability condition and subaqueous slope failure initiation. On a larger scale, comparable slope stability conditions may evolve in fjords and high-latitude ocean margins, where glacially overconsolidated deposits are overlain by postglacial (glacio-) marine sediments accumulated during deglaciation periods and by pelagic and hemipelagic sedimentation deposited during interglacials (e.g. Boe et al., 2000; Locat et al., 2003; Boe et al., 2004). Our comprehensive lake study and resulting conceptual ideas thus also improve our understanding of larger slope instabilities occurring along formerly glaciated ocean margins.

A summary list of the main conclusions includes the following:

(1) Sedimentation dominated by suspension settling from meltwater plumes, slight overconsolidation by ice-grounding and postglacial draping lead to particular slope conditions characterized by: (i) fine-grained, thinly-laminated, slightly underconsolidated Late Glacial cyclic plume deposits with low undrained shear strength values overlying (ii) overconsolidated, glacially-deformed glacial deposits with overpressured formation pore pressure. This particular succession is overlain by a Holocene drape with variable thickness that acts as a surcharge on the lower sediment layers.
(2) During past earthquake shaking, slopes that were stable under static loading conditions (FS of 1.5–2) failed along glide planes that developed at this lithological boundary.
(3) This glide plane location is a consequence of the comparably low strength conditions within the overlying thinly-laminated Late Glacial clays and the additional excess in situ pore pressure in the underlying overconsolidated, low permeable material reducing effective strength at and below the zone of failure.
(4) Limit equilibrium back-analysis reveal seismic peak ground accelerations (PGA) at the study sites of ~0.08 g (range of uncertainty ~0.02 to 0.12 g) and ~0.14 g (range of uncertainty ~0.06 to 0.16 g) for the historical 1601 A.D. M_w ~6.2 earthquake and a prehistoric, 2220 cal yr B.P., M_w>6.5 northern alpine earthquake, respectively.
(5) The results thus pinpoint the potential of detailed subaqueous slope stability analysis as paleoseismological tool that allow for quantitative reconstruction of past earthquake shaking.
(6) Holocene sedimentation rates are a key parameter in "charging" subaqueous slopes susceptible for sliding. Stability conditions thus may change over relative short geological time scales.
(7) Lessons learned from the high-resolution case studies presented here should be implemented in future studies on a basinwide scale. In combination with more detailed analysis on the dynamic behavior of the material under cyclic loading these results eventually will yield strong arguments in identifying sites of potential slope instability in the future.

Acknowledgments

We thank B. Dürr, R. Hofmann and M. Lange as well as the whole ETH-Limnoteam and friends for technical support and assistance during the campaigns, respectively. Many thanks also to Urs Gerber for the core photographs. E. Button, E. Chapron, W. Haeberli, T. Mörz, A. Puzrin, M. Schnellmann, S. Springman and S. Wiemer, are acknowledged for the numerous discussions of the methods and data presented. We thank reviewers M. De Batist and N. Sultan for thoughtful comments that considerably improved the manuscript. Accommodations and harbour for field work were kindly provided by the Swiss EAWAG Limnological Research Center at Kastanienbaum. This study was supported by the Swiss National Science Foundation (Grant 620-066113) and the Deutsche Forschungsgemeinschaft (financial support to RCOM, project C8).

References

Aeschbach-Hertig, W., 1994. Helium und Tritium als Tracer für physikalische Prozesse in Seen. PhD Thesis, ETH Zurich Nr. 10714, 272 pp.

Andrews, D.C.A., Martin, G.R., 2000. Criteria for liquefaction of silty soils. 12th World Conference on Earthquake Engineering, Proceedings, Auckland, New Zealand.

Anselmetti, F.S., Bühler, R., Finger, D., Girardclos, S., Lancini, A., Rellstab, C., Sturm, M., in press. Effects of Alpine hydropower dams on particle transport and lacustrine sedimentation. Aquat. Sci. in press.

Azizian, A., Popescu, R., 2006. Three-dimensional seismic analysis of submarine slopes. Soil Dyn. Earthqu. Eng. 26, 870–887.

Bay, F., Wiemer, S., Fäh, D., Giardini, D., 2005. Predictive ground motion scaling in Switzerland: best estimates and uncertainties. J. Seismol. 9, 223–240.

Beck, C., Van Rensbergen, P., De Batist, M., Berthier, F., Lallier, S., Manalt, F., 2001. The Late Quaternary sedimentary infill of Lake

Annecy (northwestern Alps): an overview from two seismic-reflection surveys. J. Paleolimnol. 25, 149–161.
Biscontin, G., Pestana, J.M., Nadim, F., 2004. Seismic triggering of submarine slides in soft cohesive soil deposits. Mar. Geol. 203, 341–354.
Blass, A., Anselmetti, F.S., Ariztegui, D., 2003. 60 yr of glaciolacustrine sedimentation in Steinsee (Sustenpass, Switzerland) compared with historic events and instrumental meteorological data. Eclogae Geol. Helv. 96, 59–71.
Boe, R., Hovland, M., Instanes, A., Rise, L., Vasshus, S., 2000. Submarine slide scars and mass movements in Karmsundet and Skudenesfjorden, southwestern Norway: morphology and evolution. Mar. Geol. 167, 147–165.
Boe, R., Longva, O., Lepland, A., Blikra, L.H., Sonstegaard, E., Haflidason, H., Bryn, P., Lien, R., 2004. Postglacial mass movements and their causes in fjords and lakes in western Norway. Norw. J. Geol. 84, 35–55.
Bührer, H., Ambühl, H., 1996. Der Vierwaldstättersee 1961– 1992– Eine Dokumentation. Schriftenreihe der EAWAG, vol. 10. 54 pp.
Chapron, E., Beck, C., Pourchet, M., Deconinck, J.F., 1999. 1822 earthquake-triggered homogenite in Lake Le Bourget (NW Alps). Terra Nova 11, 86–92.
Cysat, R., 1601. Collectanea Chronica und denkwürdige Sachen pro Chronica Lucernensi et Helvetiae. In: Schid, J. (Ed.), Quellen und Forschungen zur Kulturgeschichte von Luzern und der Innerschweiz. Diebold Schilling Verlag, Luzern, pp. 882–888.
Duncan, J.M., 1996. State of the art: limit equilibrium and finite-element analysis of slopes. J. Geotech. Geoenviron. Eng. 122, 577–596.
Evans, J., Dowdeswell, J.A., Grobe, H., Niessen, F., Stein, R., Hubberten, H.W., Whittington, R.J., 2002. Later Quaternary sedimentation in Kejser Franz Joseph Fjjord and the continental margin of East Greenland. In: Dowdeswell, J.A., Cofaigh, C.O. (Eds.), Glacier-Influenced Sedimentation on High-Latitude Continental Margins. Geol. Soc. London, Special Publication. The Geol. Soc. London, London, pp. 149–179.
Eyles, N., Boyce, J.I., Halfman, J.D., Koseoglu, B., 2000. Seismic stratigraphy of Waterton Lake, a sediment-starved glaciated basin in the Rocky Mountains of Alberta, Canada and Montana, USA. Sediment. Geol. 130, 283–311.
Finckh, P., Kelts, K., Lambert, A., 1984. Seismic stratigraphy and bedrock forms in perialpine lakes. Geol. Soc. Amer. Bull. 95, 1118–1128.
Florineth, D., Schluchter, C., 1998. Reconstructing the Last Glacial Maximum (LGM) ice surface geometry and flowlines in the central Swiss Alps. Eclogae Geol. Helv. 91, 391–407.
Fredlund, D.G., Krahn, J., 1977. Comparison of slope stability methods of analysis. Can. Geotech. J. 14, 429–439.
Giardini, D., Wiemer, S., Fäh, D., Deichmann, N., 2004. Seismic Hazard Assessment of Switzerland, Swiss Seismological Service, ETH Zürich. http://www.earthquake.ethz.ch/research/Swiss_Hazard/Swiss_Hazard/downloads/Hazard_report_2004.pdf.
Gisler, M., Fäh, D., Kästli, P., 2004. Historical seismicity in Central Switzerland. Eclogae Geol. Helv. 97, 221–236.
Gyger, M., Mueller-VonMoos, M., Schindler, C., 1976. Untersuchungen zur Klassifikation spaet-und nacheiszeitlicher Sedimente aus dem Zuerichsee. Schweiz. Mineral. Petrogr. Mitt. 56, 387–406.
Haeberli, W., Schlüchter, C., 1987. Geological evidence to constrain modelling of the Late Pleistocene Rhonegletscher, Swiss Alps. The Physical Basis of Ice Sheet Modelling. Proc. of the Vancouver Symposium, Vancouver, pp. 333–346.
Hampton, M.A., Lee, H.J., Locat, J., 1996. Submarine landslides. Rev. Geophys. 34, 33–59.
Hantke, R., 2003. Unterseeische Moränen im Vierwaldstätter See. In: Lienert, S. (Ed.), Geologie und Geotope im Kanton Schwyz. Schwyzerische Naturforschende Gesellschaft, Einsiedeln, pp. 106–109.
Institute, B.S., 1977. Methods of testing soil for civil engineering purposes, BS 1377. BSI, London.
Ivy Ochs, S., Schafer, J., Kubik, P.W., Synal, H.A., Schlüchter, C., 2004. Timing of deglaciation on the northern Alpine foreland (Switzerland). Eclogae Geol. Helv. 97, 47–55.
Kelts, K., 1978. Geological and Sedimentary Evolution of Lake Zurich and Zug, Switzerland. PhD Thesis, ETH, Zurich, 224 pp.
Kelts, K., 1998. Components in Lake sediments: Smear Slide Identifications. http://lrc.geo.umn.edu/smears/smsl.html.
Kelts, K., Briegel, U., Ghilardi, K., Hsu, K., 1986. The Limnogeology–ETH Coring System. Swiss J. Hydrol. 48, 104–115.
Kopp, J., 1938. Der Einfluss des Kriensbaches auf die Gestaltung des Luzernersees und die Hebung des Seespiegels des Vierwaldstättersees. Eclogae Geol. Helv. 31, 376–378.
Kramer, S.L., 1996. Geotechnical Earthquake Engineering. Prentice Hall, New Jersey. 653 pp.
Lambe, T.W., Whitman, R.V., 1979. Soil Mechanics, SI Version. John Wiley & Sons, Singapore. 553 pp.
Lee, H.J., 2005. Undersea landslides: extent and significance in the Pacific Ocean, an update. Nat. Hazards Earth Syst. Sci. 5, 877–892.
Lee, H.J., Edwards, B.D., 1986. Regional method to assess offshore slope stability. J. Geotech. Geoenviron. Eng. 112, 486–509.
Lemcke, G., 1992. Ablagerungen aus Extremereignissen als Zeitmarker der Sedimentationsgeschichte im Becken von Vitznau/Weggis (Vierwaldstättersee, Schweiz). MS thesis Thesis, Georg-August-Universtität Götting, Götting, 154 pp.
Leroueil, S., Vaunat, J., Picarelli, L., Locat, J., Lee, H.J., Faure, R., 1996. Geotechnical characterization of slope movements. Proc. Int. Symposium on Landslides, Trondheim, pp. 53–74.
Leynaud, D., Mienert, J., Nadim, F., 2004. Slope stability assessment of the Helland Hansen area offshore the mid-Norwegian margin. Mar. Geol. 213, 457–480.
Lister, G.S., 1988. A 15,000-yr isotopic record from Lake Zuerich of deglaciation and climatic change in Switzerland. Quat. Res. 29, 129–141.
Lister, G.S., Giovanoli, F., Eberli, G., Finckh, P., Finger, W., He, Q., Heim, C., Hsu, K.J., Kelts, K., Peng, C., Sidler, C., Zhao, X., 1984. Late Quaternary sediments in Lake Zurich, Switzerland. Environ. Geol. 5, 191–205.
Locat, J., Lee, H.J., 2002. Submarine landslides: advances and challenges. Can. Geotech. J. 39, 193–212.
Locat, P., Leroueil, S., Locat, J., Duchesne, M.J., 2003. Characterisation of submarine flow-slide at Pointe-Du-Fort, Saguenay Fjord, Quebec, Canada. In: Locat, J., Mienert, J. (Eds.), Submarine Mass Movements and their Consequences, pp. 521–529.
Lu, T.S., Bryant, W.R., 1997. Comparison of vane shear and fall cone strengths of soft marine clay. Mar. Georesour. Geotechnol. 15, 67–82.
Lunne, T., Robertson, P.K., Powell, J.J.M., 1997. Cone Penetration Testing in Geotechnical Practice. Spon Press. 312 pp.
Lysa, A., Sejrup, H.P., Aarseth, I., 2004. The Late Glacial–Holocene seismic stratigraphy and sedimentary environment in Ranafjorden, northern Norway. Mar. Geol. 211, 45–78.
Mackiewicz, N.E., Powell, R.D., Carlson, P.R., Molnia, B.F., 1984. Interlaminated ice-proximal glacimarine sediments in muir inlet, Alaska. Mar. Geol. 57, 113–147.
Mienert, J., 2004. COSTA—continental slope stability: major aims and topics. Mar. Geol. 213, 1–7.

Morgenstern, N.R., 1967. In: Richards, A.F. (Ed.), Submarine Slumping and Initiation of Turbidity Currents. Marine Geotechnique UP, Urbana, IL, pp. 189–220.

Morgenstern, N.R., Price, V.E., 1965. Analysis of stability of general slip surfaces. Geotechnique 15, 79–93.

Nittrouer, C.A., 1999. STRATAFORM: overview of its design and synthesis of its results. Mar. Geol. 154, 3–12.

Plötze, M., Giudici Trausch, J., Messerklinger, S., Springman, S.M., 2003. Swiss Lacustrine clay: mineralogical and mechanical characteristics. In: Cudny, K.A. (Ed.), Int. Workshop on Geotechnics of Soft Soils— Theory and Practice, Noordwijkerhout, pp. 473–478.

Quigley, R.M., Ogunbadejo, T.A., 1972. Clay layer fabric and oedometer consolidation of soft varved clay. Can. Geotech. J. 9, 165–175.

Rothwell, R.G., 1989. Minerals and Mineraloids in Marine Sediments: An Optical Identification Guide. Elsevier Appl. Sci., London. 279 pp.

Schnellmann, M., Anselmetti, F.S., Giardini, D., McKenzie, J.A., Ward, S.N., 2002. Prehistoric earthquake history revealed by lacustrine slump deposits. Geology 30, 1131–1134.

Schnellmann, M., Anselmetti, F.S., McKenzie, J.A., Giardini, D., 2005. Mass movement-induced fold-and-thrust belt structures in unconsolidated sediments in Lake Lucerne (Switzerland). Sedimentology 52, 271–289.

Schnellmann, M., Anselmetti, F.S., McKenzie, J.A., Giardini, D., 2006. 15,000 yr of mass-movement history in Lake Lucerne: implications for seismic and tsunami hazards. Eclogae Geol. Helv. 99. doi:10.1007/s00015-006-1196-7.

Schwarz-Zanetti, G., Deichmann, N., Fäh, D., Giardini, D., Jimenez, M.J., Masciadri, V., Schibler, R., Schnellman, M., 2003. The earthquake in Unterwalden on September 18, 1601: a historic-critical macroseismic evaluation. Eclogae Geol. Helv. 96, 441–450.

Shilts, W.W., Clague, J.J., 1992. Documentation of earthquake-induced disturbance of lake-sediments using subbottom acoustic profiling. Can. J. Earth Sci. 29, 1018–1042.

Siegenthaler, C., Finger, W., Kelts, K., Wang, S., 1987. Earthquake and seiche deposits in Lake Lucerne, Switzerland. Eclogae Geol. Helv. 80, 241–260.

Stegmann, S., Villinger, H., Kopf, A., 2006. Design of a modular, marine free-fall cone penetrometer. Sea Technol. 47, 27–33.

Stegmann, S., Strasser, M., Anselmetti, F.S., Kopf A., in press. Geotechnical *in situ* characterisation of subaquatic slopes: the role of pore pressure transients versus frictional strength in landslide initiation. Geophys. Res. Lett.

Strasser, M., Anselmetti, F.S., Fäh, D., Giardini, D., Schnellman, M., 2006. Magnitudes and source areas of large prehistoric northern Alpine earthquakes revealed by slope failures in lakes. Geology 34, 1005–1008.

Sturm, M., Matter, A., 1978. Turbidites and varves in Lake Brienz (Switzerland); deposition of clastic detritus by density currents. In: Matter, A., Tucker, M.E. (Eds.), Modern and Ancient Lake Sediments; Proceedings of a Symposium. Oxford International, Blackwell, pp. 147–168.

Sultan, N., Cochonat, P., Canals, M., Cattaneo, A., Dennielou, B., Haflidason, H., Laberg, J.S., Long, D., Mienert, J., Trincardi, F., 2004. Triggering mechanisms of slope instability processes and sediment failures on continental margins: a geotechnical approach. Mar. Geol. 213, 291–321.

Terzaghi, K., 1925. Erdbaumechanik. Deuticke, Wien. 399 pp.

Terzaghi, K., Peck, R.B., Mesri, G., 1996. Soil Mechniscs in Engineering practice: Chapter 16: compressibility of confined layers of soil, Third ed. New York. 549 pp.

Thevenon, F., Anselmetti, F.S., Schnellmann, M., submitted for publication. 7200 yr of human impact evidenced by automated image analysis of pyrogenic products from Lake Lucerne sediments (Central Switzerland). Quat. Sci. Rev.

Urgeles, R., Leynaud, D., Lastras, G., Canals, M., Mienert, J., 2006. Back-analysis and failure mechanisms of a large submarine slide on the ebro slope, NW Mediterranean. Mar. Geol. 226, 185–206.

Van Rensbergen, P., De Batist, M., Beck, C., Chapron, E., 1999. High-resolution seismic stratigraphy of glacial to interglacial fill of a deep glacigenic lake: Lake Le Bourget, Northwestern Alps, France. Sediment. Geol. 128, 99–129.

Waldmann, N., Ariztegui, D., Anselmetti, F.S., Austin Jr., J.A., Dunbar, R., M. Moy, C.M., Recasens, C., submitted for publication. Lago Fagnano (Tierra del Fuego, Argentina) — a continuous archive of paleoclimatic change and tectonic activity since the Late Glacial. Geologica Acta.

Wessels, M., 1998. Natural environmental changes indicated by Late Glacial and Holocene sediments from Lake Constance, Germany. Palaeogeogr. Palaeoclimatol. Palaeoecol. 140, 421–432.